Biomaterials Science

ROYAL SOCIETY OF CHEMISTRY

COMMUNICATION

View Article Online
View Journal | View Issue

Cite this: *Biomater. Sci.*, 2026, **14**, 2567

Received 23rd December 2025,
Accepted 28th February 2026

DOI: 10.1039/d5bm01883h

rsc.li/biomaterials-science

Image-based single-cell isolation in high-density seeded cells using photoactivatable surfaces

Shinya Yamahira, *[a] Yuki Umeda,[a] Teruyuki Nagamune [b] and Satoshi Yamaguchi *[a]

We developed an image-based cell isolation method utilizing a photoactivatable cell anchoring surface. After microscopically imaging the cell population on the substrate, target single cells were selectively and rapidly anchored for isolation through localized light irradiation. This approach enabled precise isolation of single cells even from densely packed seeded cells. This capability for high-throughput microscopic screening of vast cell populations provides a practical means for the detection and isolation of rare cells present at extremely low frequencies. As a proof of concept, circulating tumor cells were precisely isolated from the blood sample of a tumor-bearing mouse. This method offers a robust platform for rare cell isolation from large and dense cell populations, supporting more precise applications in cell analysis, diagnostics, and personalized medicine.

Introduction

Selective manipulation of individual cells is becoming increasingly important in various biomedical fields, including fundamental cell biology,[1–3] diagnostics,[4–7] and personalized medicine.[8,9] In particular, single-cell analysis of rare cell types, such as circulating tumor cells (CTCs), is crucial for early cancer detection and evaluation of therapeutic responses.[10–12] This has motivated a strong demand for technologies that enable precise isolation and retrieval of specific target cells from large and heterogeneous populations and thus facilitate more detailed and comprehensive analyses.[13]

Fluorescence-activated cell sorting (FACS) and magnetic-activated cell sorting (MACS) are widely used techniques for cell isolation that rely on molecular marker-based characterization.[14–17] Although effective for high-throughput sorting, these methods often fail to distinguish cells based on more complex phenotypes, such as detailed morphology[18] or subcellular protein localization.[19] Furthermore, these techniques can only analyze simple parameters, frequently leading to false positives or negatives. Consequently, for conditions such as leukemia, myelodysplastic syndromes, and malaria infections, FACS is primarily used as a supplementary diagnostic tool, whereas definitive diagnosis relies on morphological evaluation by microscopy.[20–23] Notably, recent advances in microscopy and image processing have enabled quantitative assessment of complex cellular features, including morphology,[24–26] intracellular protein distribution,[27,28] and intercellular interactions.[29] Therefore, methods that integrate microscopy-based analysis with rapid cell retrieval capabilities hold great promise for advancing single-cell analysis technologies.

To achieve such integration, technologies employing capillary-based micromanipulators[30,31] and dielectrophoresis[32–34] are widely used for cell picking. However, owing to their limited spatial precision, these methods typically require a low cell density to reliably isolate a single cell of interest. This requirement restricts the number of cells that can be analyzed within each microscopic field of view, significantly reducing the overall screening throughput and scalability. Moreover, the operational complexity of these techniques often leads to prolonged procedures, making simultaneous isolation of multiple rare cells time-consuming.

In this study, we present a novel approach that addresses these limitations by employing a light-controllable cell-anchoring surface prepared by coating the substrate with photoactivatable polyethylene glycol (PEG)-lipid **1** (Fig. 1a),[35] which selectively anchors the cells to light-irradiated areas through interactions between the outer cell membrane and the lipid component of the material (Fig. 1b). Previously, we reported a technique that enables arbitrary cell patterning by photoactivating this surface prior to cell seeding.[36] In the present study, we demonstrate for the first time that cells can be rapidly anchored by light irradiation even after cell seeding. Accordingly, we envisioned that a single cell of interest can be

[a]*SANKEN, The University of Osaka, 8-1 Mihogaoka, Ibaraki-shi, Osaka 567-0047, Japan. E-mail: syamahira@sanken.osaka-u.ac.jp, syamaguchi@sanken.osaka-u.ac.jp*
[b]*Department of Chemistry and Biotechnology, Graduate School of Engineering, The University of Tokyo, 7-3-1 Hongo, Bunkyo-ku, Tokyo 113-8656, Japan*

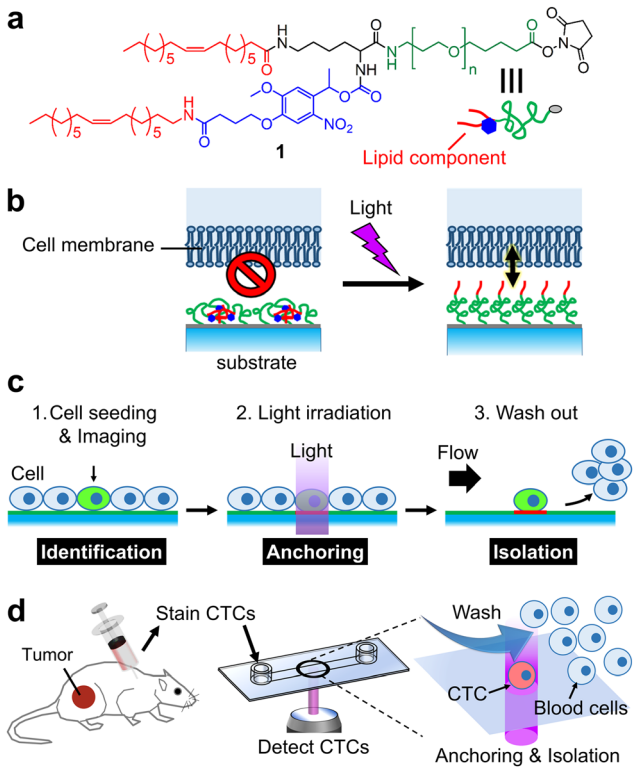

Fig. 1 (a) Chemical structure of photoactivatable PEG-lipid **1**. (b) Illustration of the surface modified with PEG-lipid **1** before and after exposure to light. (c) Schematic of light-guided cell anchoring for cell isolation after cell seeding and imaging. (d) Schematic of light-guided isolation of CTCs from the peripheral blood of a tumor-bearing mouse using microscopic identification and selective anchoring on a PEG-lipid **1**-coated microfluidic channel.

isolated through light-induced selective anchoring onto the surface after image-based analysis *via* the following three steps (Fig. 1c): (1) Target cells are identified from microscopy images; (2) owing to the high speed and spatial resolution of light irradiation, individual target cells are selectively and rapidly exposed to light spots, resulting in anchoring onto the substrate; and (3) non-anchored cells are washed away from the substrate, achieving precise isolation of the target cells. We demonstrated the effectiveness of this approach by isolating model blood cells at the single-cell level and further validated its potential clinical relevance by successfully isolating rare CTCs from blood samples obtained from tumor-bearing mice (Fig. 1d).

Experimental section

Material and reagents

Microchannels (μ-Slide VI 0.4; width: 3.8 mm, length: 17 mm, height: 0.4 mm) were purchased from Ibidi GmbH (Martinsried, Germany). The BaF3 murine pro-B cell line was obtained from RIKEN BRC (Tsukuba, Japan). BaF3 cells expressing enhanced green fluorescent protein (BaF3-EGFP) were provided by Professor Masahiro Kawahara (Kogakuin University). The DLD-1 human colonic adenocarcinoma cell line was obtained from the JCRB Cell Bank (Osaka, Japan). Calcein-AM, Cyto Red, and propidium iodide (PI) solution were purchased from Dojindo Laboratories (Kumamoto, Japan). A fatty acid-free, low-endotoxin, lyophilized powder of bovine serum albumin (BSA) was obtained from Sigma-Aldrich Co. (St Louis, MO, USA). Lymphoprep was purchased from Axis-Shield Diagnostics Ltd (Dundee, UK). Interleukin-3 (IL-3) was obtained from R&D Systems (Minneapolis, MA, USA). Qdot 655 Streptavidin Conjugate was purchased from Thermo Fisher Scientific (Waltham, MA, USA).

Ammonium–chloride–potassium (ACK) buffer was prepared by mixing NH_4Cl (8.26 g L^{-1}), K_2CO_3 (1.0 g L^{-1}), and EDTA-4Na^+ (1.0 g L^{-1}) in distilled water, followed by adjusting the pH to 7.2. Biotinylated anti-epiregulin monoclonal antibody (clone 9E5) was prepared using previously reported methods.[37,38] Briefly, 9E5 was produced from hybridoma cells implanted in BALB/c nude mice, and the resulting ascitic fluid was purified using a protein G column. The antibody was dialyzed in a boric acid buffer, biotinylated with Sulfo-NHS-LC-Biotin (EZ-Link Sulfo-NHS-LC-Biotin, Life Technologies, Carlsbad, CA, USA), and concentrated using a 100 kDa molecular weight cut-off filter.

Preparation of photoactivatable PEG-lipid 1-modified surfaces

Photoactivatable PEG-lipid **1** was synthesized using a previously reported method.[35] The plastic bottom of a commercially available microchannel was employed as the substrate. The microchannel was filled with 1% (w/v) BSA solution in phosphate-buffered saline (PBS) and incubated overnight at 4 °C. After rinsing with PBS (1 mL), a solution of 100 μM photoactivatable PEG-lipid **1** in DMSO/PBS (1 : 1, v/v) was added to the microchannel and incubated for 3–4 h at 37 °C in a humidified incubator. The reaction solution was then removed from the reservoir, and the microchannel was rinsed with PBS (1 mL).

Cell culture

BaF3, BaF3-EGFP, and DLD-1 cells were cultured in RPMI-1640 medium supplemented with 10% fetal bovine serum (FBS), 100 U mL^{-1} penicillin, and 100 μg mL^{-1} streptomycin at 37 °C in a humidified atmosphere containing 5% CO_2 and 95% air. BaF3 and BaF3-EGFP were supplemented with 1 ng mL^{-1} IL-3.

Light-induced cell anchoring onto the substrates

BaF3 cells were seeded onto the PEG-lipid-modified bottom substrate of the microchannel by introducing a BaF3 cell suspension (3×10^7 cells per mL) through the inlet. The bottom substrate was irradiated with 405 nm light at a dose of 5 J cm^{-2} to evaluate cell anchoring and at various doses ranging from 1 to 20 J cm^{-2} to assess the dose dependence, using an ultraviolet (UV) irradiator (REX-250, Asahi Spectra Co., Ltd, Tokyo, Japan) equipped with a cylindrical lens and a band-pass filter (405 ± 5 nm), followed by 10 min of incubation and

PBS rinsing. Seeded cells were observed under a fluorescence microscope (IX83; Olympus Corporation, Tokyo, Japan) before and after incubation. Cell density was quantified by image analysis using Fiji (ImageJ distribution; version 2.14.0/1.54f, NIH, Bethesda, MD, USA) with the TrackMate plugin. Cell viability was examined by live/dead staining with calcein-AM and PI following the manufacturer's instructions. Briefly, the cells were incubated with 1 μg mL^{-1} Calcein-AM and 2 μg mL^{-1} PI for 30 min at 37 °C, followed by fluorescence imaging.

Time-course analysis of light-induced cell anchoring

BaF3-EGFP cells were seeded as described above. The cell-seeded surface was irradiated with a 405 nm laser using a vertical line scan that moved from right to left across the field of view at a speed of approximately 8 μm s^{-1} with a confocal microscope (LSM 510, Carl Zeiss Microscopy GmbH, Jena, Germany). Immediately after scanning, the surface was rinsed with PBS, and green fluorescence images of the surface were acquired using the same microscope. The cell density was quantified as described above. The time-dependent anchoring of cells onto the photoactivatable surface was quantitatively analyzed using a three-state transition model. The temporal change in the density of trapped cells, $Q(t)$, was fitted using the following eqn (1):

$$Q(t) = Q_{\max}\left(1 - \frac{k_2}{k_2 - k_1}\exp(-k_1 t) + \frac{k_1}{k_2 - k_1}\exp(-k_2 t)\right) \quad (1)$$

where $Q(t)$ is the density of the trapped cells at time t, $Q_{\max}$ is the maximum density of the trapped cells, and k_1 and k_2 are the fitting parameters corresponding to the two successive steps in the three-state transition model. The experimental data were fitted to this model by nonlinear fitting of the time-course cell density data to a three-state transition model using the R software (version 4.2.1).

Preparation of PBMCs

Peripheral blood was collected in a 5 mL EDTA-2Na-containing vacutainer. Lymphoprep (4.5 mL) was added to a SepMate-15 tube (VERITAS, Tokyo, Japan) and briefly centrifuged to remove air bubbles. Peripheral blood (4 mL) was mixed with 2% (v/v) FBS (4 mL) in PBS in a 15 mL tube and then gently layered into a SepMate-15 tube. The tube was centrifuged at 1200*g* for 10 min at room temperature, and the plasma and platelet layers were discarded, leaving the peripheral blood mononuclear cell (PBMC) layer intact. The PBMC-containing supernatant was transferred to a fresh tube, mixed with 2% FBS/PBS to a final volume of 14 mL, and centrifuged at 300*g* for 10 min. The supernatant was removed, and the PBMCs were resuspended in ACK buffer to a final volume of 14 mL, followed by incubation for 10 min at room temperature for red blood cell lysis. The sample was then centrifuged, and the supernatant was discarded. The cells were resuspended in PBS for counting and centrifuged again, and the supernatant was removed and resuspended in PBS.

Light-induced selective single-cell anchoring

A subset of PBMCs was stained with calcein-AM and mixed at a ratio of approximately 1 stained cell to 10 000 unstained PBMCs. The resulting cell suspension was loaded into a microchannel containing a PEG-lipid-modified bottom substrate. The cell density was 1.6×10^4 cells per mm^2. The seeded cells covering the entire bottom surface were scanned using a confocal microscope, after which the stained cells were selectively exposed to a focused laser spot for 10 ms in the bleaching mode of the confocal microscope (TCS SP8, Leica Microsystems, Wetzlar, Germany). After approximately 200 s, the surface was rinsed under laminar PBS flow. Similarly, two subsets of BaF3 cells were stained with Calcein-AM and CytoRed. These two subsets were then mixed at a ratio of one CytoRed-stained cell to 1000 Calcein-AM-stained cells. The mixture was loaded into the microchannel. Following microscopic observation, CytoRed-stained cells within the same frame were simultaneously exposed to the laser spots, followed by rinsing.

Isolation of mouse peripheral blood and staining of CTCs

DLD-1 cells (1×10^6) were harvested by trypsinization and resuspended in a solution (200 μL) containing 50% PBS and 50% phenol red-free Matrigel (Corning, New York, USA). The cell suspension was injected subcutaneously into the right flank of male BALB/c nu/nu mice (Japan Charles River Laboratories, Tsukuba, Japan). Five weeks after tumor cell injection, peripheral blood (500 μL) was collected from the mouse by cardiac puncture using a heparin-coated syringe under isoflurane anesthesia. Subsequently, ACK buffer (4.5 mL) was added to the blood sample, and the mixture was incubated for 30 min. After two centrifugation washes and resuspension in PBS, the cells were treated with a biotinylated anti-epiregulin antibody (clone 9E5, final concentration: 100 nM) for 15 min, followed by staining with streptavidin-conjugated Qdot 655 (final concentration: 10 nM) for 5 min. After two additional washes by centrifugation and resuspension in PBS, the cells were suspended in PBS (100 μL).

The blood samples were loaded into a microchannel with a PEG-lipid-modified bottom substrate. All cells on the surface were observed *via* automatic tile-scan imaging using a confocal microscope (LSM 510; Carl Zeiss Microscopy GmbH, Jena, Germany). Individual CTCs were selectively exposed to laser spots using the region of interest (ROI) function of a confocal microscope with a 405 nm laser.

Results and discussion

Light-induced anchoring of seeded non-adherent cells

We investigated the light-induced anchoring of cells onto the PEG-lipid-modified surfaces following seeding and imaging. BaF3 cells were used as a model for non-adherent cells to minimize the influence of intrinsic cellular adhesion. In this study, a microchannel system was employed to precisely evaluate selective cell anchoring on the substrate surface, as

described in our previous work.[35,39–41] In this system, the cells on the surface were uniformly rinsed under laminar flow, allowing cells that are only weakly adhered due to nonspecific interactions to be removed. Immediately after cell seeding onto the bottom substrate of the microchannel, the surface was microscopically observed to be filled with cells (Fig. 2a). Subsequently, the designated area of the surface was irradiated with light, and after incubation to allow anchoring, non-anchored cells were washed away by rinsing. Similar features were observed in the vicinity of the boundary between the irradiated and nonirradiated areas. A high cell density was observed in the irradiated region, whereas no cells were observed in the non-irradiated region (Fig. 2b). These results clearly demonstrated that the cells were anchored onto the surface in a light-dependent manner even after seeding.

Next, we examined the effect of the light dose on cell anchoring and viability. Fig. 2c shows the density of the remaining cells on the surfaces irradiated with various light doses. At doses above 5 J cm^{-2}, a high cell density remained, whereas only a few cells remained at doses below 2 J cm^{-2}. Additionally, the cell density remained essentially constant when the light dose was increased from 5 to 20 J cm^{-2}. Based on these results, we conclude that a light dose of 5 J cm^{-2} is sufficient for cell anchoring. The viabilities of the remaining cells were examined under the same conditions. The results showed that the proportion of viable cells did not change following irradiation with light doses between 2 and 20 J cm^{-2} (Fig. 2c). These findings indicate that cells can be anchored to a photoactivatable surface using biocompatible levels of light exposure. The remaining cells proliferated (SI Fig. S1). Thus, the present photoactivatable surface enables light-induced selective anchoring of viable cells. Nevertheless, at the molecular level, potential transcriptional effects induced by light irradiation, which may be relevant for transcriptome-sensitive downstream analyses, cannot be excluded and are therefore noted as a limitation of the present study and an important direction for future investigation. In addition, to clarify whether the present isolation protocol is compatible with fixed cells, the same experiments were performed using paraformaldehyde-fixed cells. Compared with living cells, fixed cells exhibited markedly reduced capture efficiency (see SI Fig. S2), suggesting that efficient anchoring depends on the properties of the live cell membrane.

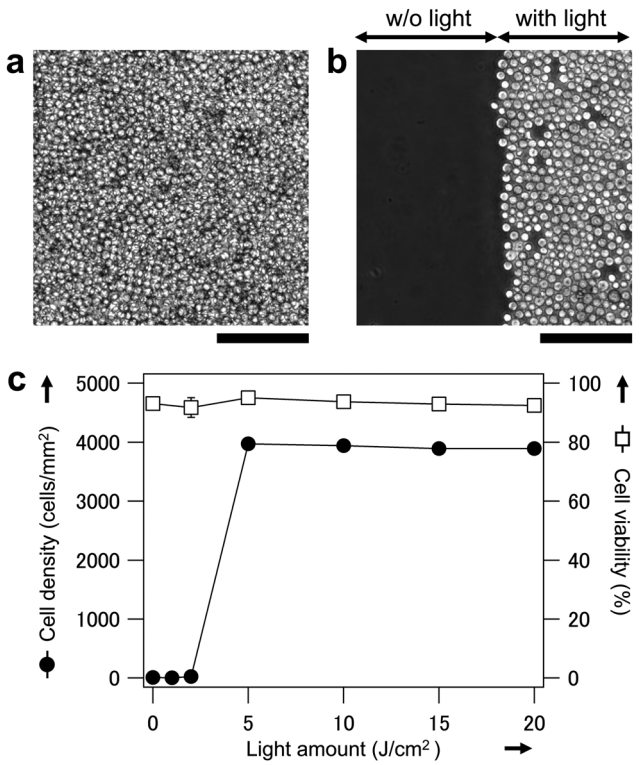

Fig. 2 Light-induced anchoring of seeded floating cells on the PEG-lipid-modified surface. (a) Cells immediately after seeding onto the PEG-lipid-modified substrate. (b) Light-guided selective anchoring, with cells remaining only in the irradiated region after rinsing. (c) Anchored cell density (black circles, left axis) and cell viability (open squares, right axis) plotted against the light dose (n = 3).

Time-course analysis of light-induced cell anchoring

We investigated the time required for cell anchoring after light exposure. To analyze the kinetics of cell anchoring, the cell-seeded surface was irradiated with laser light using a vertical line scan from right to left across the field of view, followed by immediate rinsing with PBS (Fig. 3a). In this protocol, the right side of the surface underwent a longer incubation period between light irradiation and rinsing than the left side, generating a gradient of incubation times ranging from 14 to 361 s across the surface (Fig. 3b). Upon light irradiation, the density of the anchored BaF3-EGFP, as visualized by fluorescence, increased with longer incubation times (Fig. 3b). The images were analyzed by counting the number of anchored cells, and the cell densities were plotted *versus* the incubation time (Fig. 3c). Cell anchoring on this surface consists of two major steps: photo-induced activation of PEG-lipids upon light irradiation, followed by interactions between the activated PEG-lipids and the cell membrane. Accordingly, fitting the data with a three-state transition model yielded phenomenological characteristic time scales of 53 s and 31 s for the respective steps, with saturation occurring at approximately 300 s. These results indicate that cell anchoring on the photoactivatable surface proceeded rapidly within a few minutes.

Light-induced selective single-cell isolation

We performed light-induced selective anchoring of individual target cells using a photoactivatable surface. Human PBMCs were used as a medically relevant model cell type. A cell suspension containing approximately 0.01% green fluorescently stained cells was loaded into the microchannel with a PEG-lipid-modified bottom substrate. Among the seeded cells covering the entire bottom surface, the stained cells were identified by confocal microscopy (Fig. 4a). Subsequently, under microscopic observation, the stained cells were selectively exposed to a focused light spot for anchoring, followed by rinsing with laminar PBS flow to remove the non-anchored

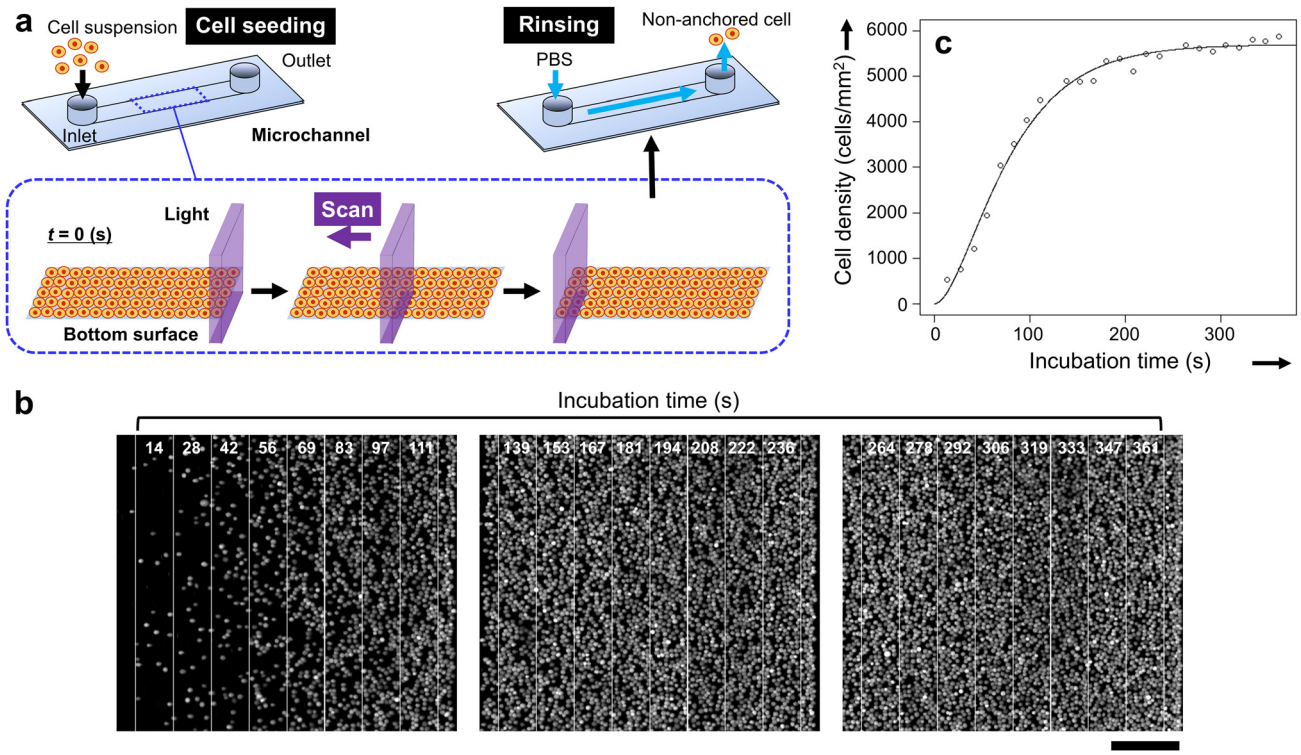

Fig. 3 Light-induced anchoring of floating cells seeded on the PEG-lipid-modified surface. (a) Schematic of the experimental system. (b) Fluorescence images of BaF3-EGFP cells on the PEG-lipid-modified surface after line-scanning irradiation with a 405 nm laser from right to left and subsequent rinsing. Each irradiated region separated by white lines was incubated for an average of (left panel) 14–111 s, (middle panel) 139–236 s, and (right panel) 264–361 s before rinsing. Scale bar, 200 μm. (c) Density of anchored cells plotted as a function of the time interval between light irradiation and rinsing. The data were fitted using a three-state transition model.

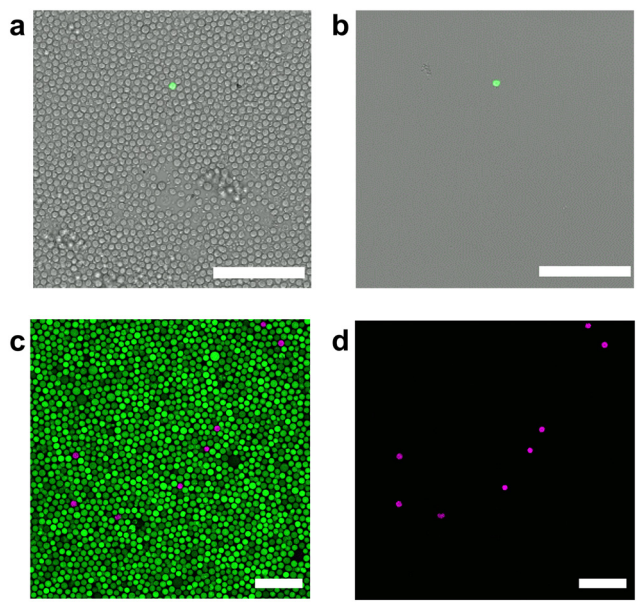

Fig. 4 Light-induced selective anchoring of single cells. (a) Fluorescence and bright-field merged image of the seeded PBMCs before and (b) after selective light irradiation of a green fluorescence-stained cell followed by rinsing. Scale bar, 100 μm. (c) Fluorescence image of BaF3 cells stained with green fluorescence and red fluorescence (displayed as magenta in pseudo-color) before and (d) after selective light irradiation of red fluorescence-stained cells and rinsing. Scale bar, 100 μm.

unstained cells. Only stained cells remained anchored and immobile, whereas the surrounding unstained cells were rapidly removed (see SI, Movie S1). Thus, a rare, individual target blood cell was accurately isolated on the substrate surface from a densely packed population in which the cells were in close contact with one another (Fig. 4b).

Multiple cells of interest were simultaneously isolated from the photoactivatable surface. Two subsets of BaF3 cells were stained with red and green fluorescent dyes, mixed, and loaded into the microchannel at high density (Fig. 4c). After scanning the cell-seeded surface, the red fluorescently stained cells were selectively exposed to laser spots with an irradiation time of 4 ms per cell. After rinsing, all eight red fluorescently stained cells remained on the surface, whereas no green fluorescently stained cells remained (Fig. 4d). Across three independent experiments, 27 target cells were exposed to focused light spots, of which 24 were successfully isolated. Only one case resulted in the co-capture of an adjacent off-target cell, while in three cases the target cells did not remain on the surface (Fig. 4d and SI, Fig. S3). Despite these minor mismatches arising from manual laser spot positioning and focusing, consistent isolation performance was achieved, indicating that isolation precision could be further improved through automation of laser irradiation control.

Live cell-staining dyes were applied, and all isolated cells retained their fluorescence signals, confirming their viability.

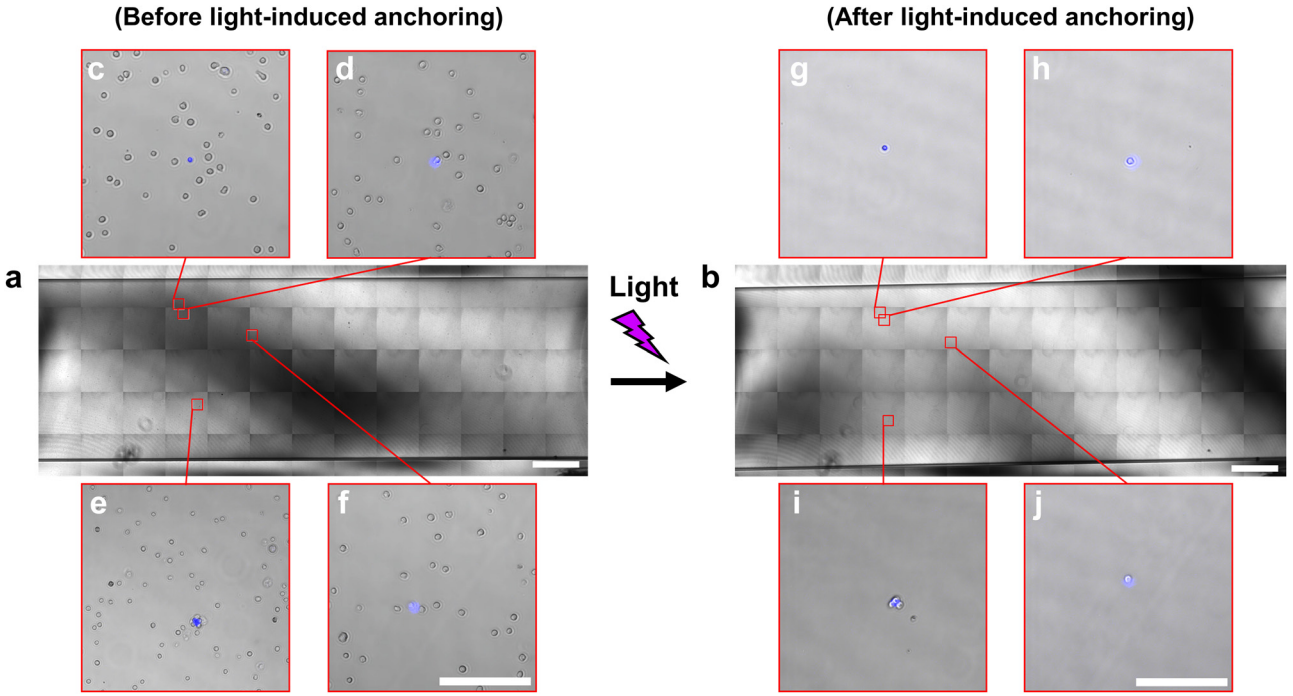

Fig. 5 Light-induced selective anchoring of circulating tumor cells from a blood sample. (a) Confocal tile-scan image over the entire bottom surface of a microchannel before and (b) after light irradiation and subsequent washing. Scale bar, 1 mm. (c–f) Enlarged images showing blood cells containing fluorescently stained CTCs (blue) before light irradiation. (g–j) Corresponding regions after irradiation and washing, in which only the irradiated CTCs remained anchored. Scale bar, 100 μm.

These results demonstrate that both single and multiple target cells can be isolated through rapid and simple light irradiation without significant photodamage or loss of viability. Notably, this method enables cell sorting even in high-density cell populations, overcoming the limitations of previously reported approaches, such as capillary-based micromanipulators,[29–31] optical tweezers,[42,43] acoustic tweezers,[44] and dielectrophoresis,[45–47] which typically require low-density conditions for accurate single-cell recovery and therefore are unsuitable for retrieving rare cells from large populations. Even in microwell-assisted approaches, which offer relatively high throughput and scalability compared to the conventional methods by optimizing the intercellular spacing for single-cell picking, cell isolation has previously been limited to densities of up to approximately 1000 cells per mm^2.[10,30] By contrast, the present study achieved accurate single-cell isolation at densities exceeding the conventional density limit by an order of magnitude. Thus, this method is uniquely suited for isolating rare cells from large populations without compromising cell viability.

Isolation of multiple circulating tumor cells

CTCs are tumor-derived cells that are shed into the bloodstream and enable a noninvasive liquid biopsy for cancer. Since CTCs serve as key biomarkers for cancer diagnosis and monitoring of disease progression, their reliable isolation is essential, as it enables molecular and genetic analyses to guide prognosis and treatment selection.[48–50] To address this need, we demonstrated the isolation of CTCs from peripheral blood samples using the present photoactivatable surface. Peripheral blood was collected five weeks after tumor implantation from tumor-bearing mice inoculated with human colorectal adenocarcinoma DLD-1 cells. After fluorescence immunostaining of the CTCs, the blood sample was loaded into a microchannel coated with photoactivatable PEG-lipid **1**. All cells on the surface were observed using automatic tile-scan imaging (Fig. 5a). Among these 65 images, fluorescently stained CTCs were identified in four images (Fig. 5c–f). Individual CTCs were then selectively exposed to light. In one image (Fig. 5e), three CTCs were aggregated and exposed to a larger light spot. After rinsing the surface with PBS, only the irradiated CTCs selectively remained anchored, whereas the non-irradiated blood cells were removed (Fig. 5b and g–j). These results demonstrate that clinically important rare cells such as CTCs can be precisely and efficiently isolated through light-guided *in situ* activation on this photoactivatable surface.

Conclusions

This study presents a method for light-induced selective isolation of single cells on a photoactivatable surface. By combining microscopic observations for target detection with localized light irradiation for selective anchoring, the target cells were rapidly and precisely anchored and subsequently recovered even from densely packed cultures that exceeded the density limits of conventional single-cell picking methods by

more than ten times. This capability is particularly advantageous for the detection and isolation of rare cells at extremely low frequencies, as their recovery requires high-density observations that allow rapid screening of large cell populations for which conventional isolation techniques are limited in their ability to isolate only single target cells. Additionally, multiple target cells can be recovered simultaneously within a short processing time. The accuracy and efficiency of the proposed method were attributed to the rapid and robust cell-trapping capabilities of the photoactivatable surface combined with light stimulation, which provided subcellular-resolution control and fast manipulation. CTCs, identified as aggregates through prior microscopic observations, were successfully isolated. Based on this result, this technique is expected to be applicable not only to fluorescence-based cell selection but also to the selection of cells based on more complex phenotypes, such as morphology. Overall, this light-responsive surface is a promising tool for a variety of biomedical applications and provides a new avenue for high-throughput and high-precision single-cell manipulation with the potential to revolutionize single-cell analysis and diagnostics in medical research.

Author contributions

Sh. Y., T. N. and Sa. Y. conceptualized the study. Sh. Y. and Sa. Y. designed the methodology of the study. Sh. Y. and Y. U. performed the experiments. Sh. Y., Y. U. and Sa. Y. analyzed the data. Sh. Y., T. N. and Sa. Y. supervised the study. Sh. Y. and Sa. Y. wrote the original draft of the manuscript. Sa. Y., Y. U., T. N. and Sh. Y. reviewed and edited the manuscript. Sh. Y. and Sa. Y. acquired fundings.

Conflicts of interest

A patent was granted for the technology reported in this study. The authors declare no conflict of interest.

Ethical statement

Mice were maintained in accordance with the Guide for the Care and Use of Laboratory Animals of the University of Tokyo. This study was approved by the Institutional Animal Care and Use Committee of the University of Tokyo (Permit Number: KA12-11-2) and the Institutional Review Board of St. Luke's International University (14-R158).

Data availability

The data supporting this article have been included as part of the supplementary information (SI). Supplementary information is available. Supplementary information: Fig. S1 and S3, Movie S1 and further experimental details. See DOI: https://doi.org/10.1039/d5bm01883h.

Acknowledgements

This work was supported by the Ministry of Education, Culture, Sports, Science and Technology (MEXT) of Japan, Leading Initiative for Excellent Young Researchers (LEADER) project (16812307), Fund for the Promotion of Joint International Research (International Collaborative Research) (24KK0103), Grant-in-Aid for Scientific Research (C) (22K04898), and Scientific Research (B) (24K01261). Part of this work was supported by research grants from the Uehara Memorial Foundation (202380032), Japan Science and Technology Agency (JST) PRESTO (JPMJPR16FA), the MIRAI program (JPMJMI19G6), the FOREST Program (JPMJFR244Y), and CREST (JPMJCR2434).

References

1 D. Gao, F. Jin, M. Zhou and Y. Jiang, *Analyst*, 2019, **144**, 766–781.
2 F. Guo, Z. Mao, Y. Chen, Z. Xie, J. P. Lata, P. Li, L. Ren, J. Liu, J. Yang, M. Dao, S. Suresh and T. J. Huang, *Proc. Natl. Acad. Sci. U. S. A.*, 2016, **113**, 1522–1527.
3 X. Gou, R. Wang, S. S. Y. Lam, J. Hou, A. Y. H. Leung and D. Sun, *Biomed. Eng. Online*, 2015, **14**, 114.
4 B. Zheng, C.-Y. Li, S. Huang, Z.-L. Zhang, Q.-S. Wu, D.-W. Pang and H.-W. Tang, *Sens. Actuators, B*, 2022, **368**, 132173.
5 H. Chen, S. Y. Osman, D. L. Moose, M. Vanneste, J. L. Anderson, M. D. Henry and R. K. Anand, *Lab Chip*, 2023, **23**, 2586–2600.
6 B. Dura, M. M. Servos, R. M. Barry, H. L. Ploegh, S. K. Dougan and J. Voldman, *Proc. Natl. Acad. Sci. U. S. A.*, 2016, **113**, E3599–E3608.
7 R. Negishi, H. Yamakawa, T. Kobayashi, M. Horikawa, T. Shimoyama, F. Koizumi, T. Sawada, K. Oboki, Y. Omuro, C. Funasaka, A. Kageyama, Y. Kanemasa, T. Tanaka, T. Matsunaga and T. Yoshino, *Commun. Biol.*, 2022, **5**, 20.
8 J. C. Harris, S. M. Prouty, M. A. Nelson, D. C. Sung, A. M. Nelson, J. T. Seykora, T. Kambayashi and E. A. Grice, *J. Invest. Dermatol.*, 2024, **144**, 1161–1165.
9 S. Yamamura, H. Kishi, Y. Tokimitsu, S. Kondo, R. Honda, S. R. Rao, M. Omori, E. Tamiya and A. Muraguchi, *Anal. Chem.*, 2005, **77**, 8050–8056.
10 M. Pestrin, F. Salvianti, F. Galardi, F. De Luca, N. Turner, L. Malorni, M. Pazzagli, A. Di Leo and P. Pinzani, *Mol. Oncol.*, 2015, **9**, 749–757.
11 D. J. E. Peeters, B. De Laere, G. G. Van den Eynden, S. J. Van Laere, F. Rothé, M. Ignatiadis, A. M. Sieuwerts, D. Lambrechts, A. Rutten, P. A. van Dam, P. Pauwels, M. Peeters, P. B. Vermeulen and L. Y. Dirix, *Br. J. Cancer*, 2013, **108**, 1358–1367.

12 S. J. Cohen, C. J. A. Punt, N. Iannotti, B. H. Saidman, K. D. Sabbath, N. Y. Gabrail, J. Picus, M. Morse, E. Mitchell, M. C. Miller, G. V. Doyle, H. Tissing, L. W. M. M. Terstappen and N. J. Meropol, *J. Clin. Oncol.*, 2008, **26**, 3213–3221.
13 S. Hosic, S. K. Murthy and A. N. Koppes, *Anal. Chem.*, 2016, **88**, 354–380.
14 B. D. Plouffe, S. K. Murthy and L. H. Lewis, *Rep. Prog. Phys.*, 2015, **78**, 016601.
15 T. Bexte, N. Albinger, A. Al Ajami, P. Wendel, L. Buchinger, A. Gessner, J. Alzubi, V. Särchen, M. Vogler, H. M. Rasheed, B. A. Jung, S. Wolf, R. Bhayadia, T. Oellerich, J.-H. Klusmann, O. Penack, N. Möker, T. Cathomen, M. A. Rieger, K. Imkeller and E. Ullrich, *Nat. Commun.*, 2024, **15**, 8439.
16 W. A. Bonner, H. R. Hulett, R. G. Sweet and L. A. Herzenberg, *Rev. Sci. Instrum.*, 1972, **43**, 404–409.
17 S. Miltenyi, W. Muller, W. Weichel and A. Radbruch, *Cytometry*, 1990, **11**, 231–238.
18 J. E. Henning, D. Y. Lee, R. L. Ferrante, A. S. McCallum, J. S. Walker, K. R. Kozminski, J. A. Graff, A. C. Nelson, R. A. Hughes, M. S. Calhoun, C. A. Marquez, K. M. Schleicher, D. J. O'Dell, D. K. Meyerholz, C. M. Maher, M. C. Jensen, C. L. Sompalli, P. K. Nguyen, R. D. Hume, J. E. Slansky and D. M. Kranz, *Mol. Ther.*, 2025, **33**, 1179–1193.
19 S. Yamahira, S. Yamaguchi, M. Kawahara and T. Nagamune, *Macromol. Biosci.*, 2014, **14**, 1670–1676.
20 M. Tan, S. Yamaguchi, S. Yamahira, M. Nakamura and T. Nagamune, *Lab Chip*, 2017, **17**, 1933–1938.
21 J. Wu, J. Chen, J. Wang, Y. Deng, Y. Zhou, B. Qian, J. Xu, L. Wang, W. Wang and J. Li, *BMC Bioinf.*, 2021, **22**, 349.
22 A. H. Song, M. Williams, D. F. K. Williamson, S. S. L. Chow, G. Jaume, G. Gao, A. Zhang, B. Chen, A. S. Baras, R. Serafin, R. Colling, M. R. Downes, X. Farré, P. Humphrey, C. Verrill, L. D. True, A. V. Parwani, J. T. C. Liu and F. Mahmood, *Cell*, 2024, **187**, 2502–2520.
23 J. H. Yang, Y. Kim, J. Lim, M. Kim, E.-J. Oh, H.-K. Lee, Y.-J. Park, W. S. Min, B. Cho, K. Lee and K. Han, *Ann. Clin. Lab. Sci.*, 2014, **44**, 19–26.
24 T. Shiina, K. Kimura, Y. Takemoto, K. Tanaka and R. Kato, *J. Biosci. Bioeng.*, 2025, **139**, 329–339.
25 S. Chen, M. Zhao, G. Wu, C. Yao and J. Zhang, *Comput. Math. Methods Med.*, 2012, **2012**, 101536.
26 R. Kato, M. Matsumoto, H. Sasaki, R. Joto, M. Okada, Y. Ikeda, K. Kanie, M. Suga, M. Kinehara, K. Yanagihara, Y. Liu, K. Uchio-Yamada, T. Fukuda, H. Kii, T. Uozumi, H. Honda, Y. Kiyota and M. K. Furue, *Sci. Rep.*, 2016, **6**, 34009.
27 T. C. Voss, I. A. Demarco and R. N. Day, *BioTechniques*, 2005, **38**, 413–424.
28 Y. Sun, Z. Lu, J. A. Taylor and J. L. S. Au, *J. Controlled Release*, 2024, **365**, 89–100.
29 T. Sano, T. Nakajima, K. A. Senda, S. Nakano, M. Yamato, Y. Ikeda, H. Zeng, J. Kawabe and Y. T. Matsunaga, *Stem Cell Res. Ther.*, 2022, **13**, 532.
30 N. Yoshimoto, A. Kida, X. Jie, M. Kurokawa, M. Iijima, T. Niimi, A. D. Maturana, I. Nikaido, H. R. Ueda, K. Tatematsu, K. Tanizawa, A. Kondo, I. Fujii and S. Kuroda, *Sci. Rep.*, 2013, **3**, 1191.
31 S. Yatsushiro, S. Yamamura, Y. Yamaguchi, Y. Shinohara, E. Tamiya, T. Horii, Y. Baba and M. Kataoka, *PLoS One*, 2010, **5**, e13179.
32 Z. Tian, X. Wang and J. Chen, *Microsyst. Nanoeng.*, 2024, **10**, 117.
33 K. Le, C. Tan, H. Le, J. Tat, E. Zasadzinska, J. Diep, R. Zastrow, C. Chen and J. Stevens, *Biotechnol. J.*, 2020, **15**, 1900247.
34 J. Diep, H. Le, K. Le, E. Zasadzinska, J. Tat, P. Yam, R. Zastrow, N. Gomez and J. Stevens, *Biotechnol. Prog.*, 2021, **37**, e3192.
35 S. Yamahira, R. Misawa, T. Kosaka, M. Tan, S. Izuta, H. Yamashita, Y. Heike, A. Okamoto, T. Nagamune and S. Yamaguchi, *J. Am. Chem. Soc.*, 2022, **144**, 13154–13162.
36 S. Yamahira, H. Mitsuno, M. Yamaoka, T. Nagamune, A. Okamoto, R. Kanzaki and S. Yamaguchi, *Biosens. Bioelectron.: X*, 2024, **18**, 100473.
37 Y. H. Lee, M. Iijima, Y. Kado, E. Mizohata, T. Inoue, A. Sugiyama, H. Y. Shibasaki and T. Kodama, *Biochem. Biophys. Res. Commun.*, 2013, **441**, 1011–1017.
38 A. Ishijima, K. Minamihata, S. Yamaguchi, S. Yamahira, R. Ichikawa, E. Kobayashi, M. Iijima, Y. Shibasaki, T. Azuma, T. Nagamune and I. Sakuma, *Sci. Rep.*, 2017, **7**, 44077.
39 N. T. Jarzębska, S. Yamaguchi, S. Izuta, T. Kosaka, S. Yamahira, T. Nagamune and A. Okamoto, *Biomater. Sci.*, 2020, **7**, 4514–4518.
40 T. Kosaka, S. Yamaguchi, S. Izuta, S. Yamahira, Y. Shibasaki, H. Tateno and A. Okamoto, *J. Am. Chem. Soc.*, 2022, **144**, 17980–17988.
41 Y. Umeda, S. Yamahira, K. Nakamura, T. Takagi, T. Suzuki, K. Sato, Y. Hirabayashi, A. Okamoto and S. Yamaguchi, *Lab Chip*, 2025, **25**, 2222–2233.
42 B. Landenberger, H. Höfemann, S. Wadle and A. Rohrbach, *Lab Chip*, 2012, **12**, 3177–3183.
43 H. Zhang and K.-K. Liu, *J. R. Soc., Interface*, 2008, **5**, 671–690.
44 S. Yang, J. Rufo, R. Zhong, J. Rich, Z. Wang, L. P. Lee and T. J. Huang, *Nat. Protoc.*, 2023, **18**, 2441–2458.
45 H. Hsu, A. T. Ohta, P. Chiou, A. Jamshidi, S. L. Neale and M. C. Wu, *Lab Chip*, 2010, **10**, 165–172.
46 X. Hu, P. H. Bessette, J. Qian, C. D. Meinhart, H. T. Dinh, R. P. Wang, A. B. Keeney, J. P. Andrews, P. S. Demetri and M. Toner, *Proc. Natl. Acad. Sci. U. S. A.*, 2005, **102**, 15757–15761.
47 P. Y. Chiou, A. T. Ohta and M. C. Wu, *Nature*, 2005, **436**, 370–372.
48 M. Yu, S. Stott, M. Toner, S. Maheswaran and D. A. Haber, *J. Cell Biol.*, 2011, **192**, 373–382.
49 C. Alix-Panabières and K. Pantel, *Nat. Rev. Cancer*, 2014, **14**, 623–638.
50 K. Pantel and C. Alix-Panabières, *Nat. Rev. Clin. Oncol.*, 2019, **16**, 409–424.

